the electrostatic field significantly influences the saturation pressure, but the actual electrostatic field applied by an electrostatic source is only 2000–8000 V/cm[3]. It is a well-known fact that for a uniform electrostatic field, the electric field at the tip of any rounded object inserted into the field increases significantly as the inverse of the radius, $1/r_c$, increases, where r_c is the radius of the end of the object. Babakin et al.[2] studied the relationship between the electric field and the needle frost experimentally, and found

$$K_{yc} = 1 + \frac{1}{\frac{1}{2}\sqrt{[(\eta_0 + 1)/(\eta_0 - 1)]} - (1/\eta_0)} \times \left[\frac{1}{(a/c) - (c/a)} - \frac{1}{2}\sqrt{\frac{(a/c) + 1}{(a/c) - 1}}\right] \quad (8)$$

where K_{yc} is the electric field coefficient, which is equal to the ratio of the electric field at the sharp point of the needle frost to the average uniform electric field that is applied, a is the height of the needle frost, $2b$ is the diameter of the needle frost, c is equal to $(a^2 - b^2)^{0.5}$, and η_0 is the ratio a/c. The resulting electric field can be determined from Eq. (8), and then using Eq. (7) the corresponding saturation pressure can be found. These results are listed in Table 1 where the average electric field E is assumed to be 5000 V/cm.

During the initial stage of frost formation, the frost grows very slowly both with and without an electric field. As the crystal branch grows, a sharp point appears on the end of the crystal, and as illustrated in Table 1 or Eq. (8), the electric field will increase. From Eq. (7) the saturation pressure will decrease, and the driving force of the phase change from Eq. (1) will increase significantly. Therefore, the growth of the frost crystal is accelerated. Since the gradient of the electric field is largest along the direction of the electric field, the driving force of the phase change is also the largest in this direction, and the frost grows more quickly along this axis. With the growth of frost, the ratio of the height of the frost to the diameter becomes larger, and as shown in Table 1, the electric field and the driving force of the phase change increase further, promoting continued increases in the height of the frost formation. Once the frost is formed, it will grow very rapidly along the direction of the electric field, and within a very short time will approach the long slender shape of the characteristic needle frost.

Clearly, the electrostatic field changes the saturation pressure and the driving force of the phase change, resulting in the needle frost formation. This explanation also qualitatively verifies the experimental conclusion that when the electrostatic field increases, the condensing temperature increases.[6] This also brings into question the previously offered explanation that the electric field at the surface of the crystals might be sufficient to modify the mean surface migration distance of water molecules, and hence, change the process of ice formation and growth.[6] This explanation cannot satisfactorily explain the entire growth process of ice needles under the influence of electric fields.

In the process of deriving Eq. (7), the interface energy influence is included in the term dG_σ/dm_α. Since the interface thickness is very thin and only several molecule layers thick, the Gibbs free energy is nearly equal to the interface Helmholtz energy. Following the definition of the interface free energy of vapor–liquid[7]

$$\gamma = \frac{dF_\sigma}{dA_\sigma} \quad \text{or} \quad dF_\sigma = \gamma\, dA_\sigma = \gamma 8\pi r\, dr \quad (9)$$

and considering the mass change of the ice ball, the critical radius of ice nucleation can be obtained as

$$r_c = \frac{2\gamma}{\rho_\alpha RT\sqrt{\frac{p}{p_0}} - \frac{\lambda\rho_\alpha}{R}\left(\frac{T - T_0}{T_0}\right) + \frac{\chi\varepsilon_0 E^2}{2}} \quad (10)$$

From Eq. (10), it can be shown that the critical radius of ice nucleation under the influence of an electrostatic field is smaller than when no electrostatic field is present, making it easier to form ice nuclei in the presence of electrostatic fields.

Conclusions

The fundamental thermodynamic expressions that describe the effect of electrostatic fields on the vapor–solid phase change processes occurring during frost formation have been derived in an effort to qualitatively explain some of the experimentally observed phenomenon occurring in this process. Utilizing fundamental thermodynamic principles and phase-change theory, a saturation pressure equation and an expression for the critical radius of ice nuclei under an electrostatic field were derived.

The results indicate that when the electric field increases, the saturation pressure at the surface of the needle frost and the critical radius of ice nucleation both decrease. In addition, from the perspective of phase-change dynamics, since the saturation pressure will decrease with increases in the electrostatic field, the driving force of the phase change process increases significantly and results in the needle frost formation on cooled or cryo surfaces under the influence of electrostatic fields.

References

[1]Hayashi, Y., Aoki, A., Adachi, S., and Hori, K., "Study of Frost Properties Correlating with Frost Formation Types," *Journal of Heat Transfer*, Vol. 99, No. 2, 1977, pp. 239–245.

[2]Babakin, B. C., and Elykin, M. A., "Frost Formation on the Surface of Refrigeration Apparatus under Electric Fields," *Journal of Refrigeration*, No. 2, 1985, pp. 33–37.

[3]Meng, F. J., Ma, H. B., and Pan, Y. L., "Heat Transfer Enhancement Under Frosting Conditions Through Sublimation by High Voltage Electrostatic Fields," *Heat Transfer Enhancement and Energy Conservation*, Hemisphere, New York, 1990, pp. 511–518.

[4]Halliday, D., and Resnick, R., *Physics*, Pt. 2, 3rd Ed., Wiley, New York, 1978.

[5]Brice, J. C., *Crystal Growth Processes*, Wiley, New York, 1986, pp. 61–64.

[6]Hobbs, P. V., *Ice Physics*, Clarendon, Oxford, England, UK, 1974, pp. 524–571.

[7]Carey, V. P., *Liquid-Vapor Phase-Change Phenomena*, Hemisphere, Washington, DC, 1992, pp. 25–54.

Mixed Convection in a Vertical Channel with Heated Blocks

H. H. Li* and B. T. F. Chung†
University of Akron, Akron, Ohio 44325-3903

Introduction

ALTHOUGH natural convection in heated vertical channels has been studied extensively,[1] theoretical study on mixed convection has been essentially limited to the buoyancy-aided flow.[2] Recently, Gau et al.[3] studied both buoyancy-aided and buoyancy-opposed convection in flat-plate channels. Kim and Boehm[4] considered the buoyancy-aided

Received Aug. 15, 1994; revision received Feb. 27, 1995; accepted for publication March 2, 1995.

*Graduate Assistant, Department of Mechanical Engineering. Student Member AIAA.

†F. Theodore Harrington Professor of Mechanical Engineering, Department of Mechanical Engineering.

convection in a channel with heated blocks. In the present work, mixed convection is studied numerically in a vertical channel with several uniformly heated blocks deployed on one plate. Effort is first made to distinguish between the forced fluid flow due to the external drive, and the natural fluid flow due to the chimney effect. A "natural Reynolds number" Rn, defined as the Reynolds number induced by buoyancy, is proposed for this purpose. Rn is determined by examining a pure buoyancy-driven flow (i.e., no external force). By comparing Rn with the imposed Reynolds number Re, three cases of combined forced and buoyant flow are categorized. When the forced flow is upward, buoyancy aids the flow and Re is greater than Rn. When the forced flow is downward and stronger than the opposing buoyant flow, the combined flow directs downward. However, when a downward forced flow is weaker than the opposing buoyant flow, the combined flow directs upward, but Re is less than Rn. This last case is unique for the heated channel and it occurs due to the chimney effect.

Numerically, the present problem involves unknown entrance velocity, especially when a flow reversal occurs in the passage. A calculation presuming the entrance velocity profile is no longer suitable. Therefore, a special numerical formulation is designed in this study. The obtained results show the importance of the parameter Ra/Re^2 in its role to govern the heat transfer mechanisms.

Mathematical Formulation

The geometry under consideration is shown in Fig. 1. The flow is assumed to be two-dimensional, laminar, incompressible with negligible viscous dissipation. Flow at the entrance is assumed fully developed. The properties of materials are constant. The dimensionless governing equations are written by invoking the Boussinesq's approximation.

$$\frac{\partial u}{\partial x} + \frac{\partial v}{\partial y} = 0 \tag{1}$$

$$\frac{\partial u}{\partial t} + u\frac{\partial u}{\partial x} + v\frac{\partial u}{\partial y} = \frac{1}{Re}\left(\frac{\partial^2 u}{\partial x^2} + \frac{\partial^2 u}{\partial y^2}\right) - \frac{\partial p}{\partial x} \pm \frac{Ra}{PrRe^2}\theta \tag{2}$$

$$\frac{\partial v}{\partial t} + u\frac{\partial v}{\partial x} + v\frac{\partial v}{\partial y} = \frac{1}{Re}\left(\frac{\partial^2 v}{\partial x^2} + \frac{\partial^2 v}{\partial y^2}\right) - \frac{\partial p}{\partial y} \tag{3}$$

$$\frac{\partial \theta}{\partial t} + u\frac{\partial \theta}{\partial x} + v\frac{\partial \theta}{\partial y} = \frac{\eta}{PrRe}\left(\frac{\partial^2 \theta}{\partial x^2} + \frac{\partial^2 \theta}{\partial y^2}\right) + \frac{q}{PrRe} \tag{4}$$

where η is the ratio of thermal diffusivity, i.e., $\eta = \alpha/\alpha_f$. In our problem, $\eta = 4.0$ in blocks and $\eta = 1.0$ in fluid. q in the heat source term equals $1/wh$ in the blocks and zero in fluid, with w and h defined in Fig. 1. p is the effective pressure absorbing in the hydrostatic pressure. The buoyancy term takes a positive sign for upward flow and negative for downward flow. The unsteady terms are included since the pseudotransient method is employed to solve the steady-state problem. The scales used to normalize the above equations are the channel width, mean axial velocity, and the volumetric heat generation in the blocks.

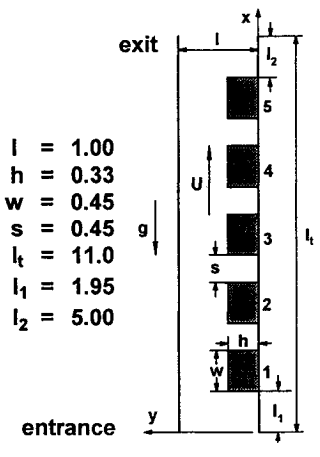

Fig. 1 Vertical channel with five heat generating blocks asymmetrically deployed.

A numerical procedure combining the SIMPLE[5] algorithm with the QUICK[6] scheme is adopted to solve the above equations. While the flow is solved in the fluid region only, the temperature field is solved conjugately in both fluid and the blocks. Flow boundary conditions are $u = 0$, $v = 0$ on the solid surface, $\partial u/\partial x = 0$, $\partial v/\partial x = 0$, $p = p_i$ at the entrance, and $\partial u/\partial x = 0$, $\partial v/\partial x = 0$, $p = p_0$ at the exit. For given Re and Ra, the pressure difference between the entrance and the exit is adjusted so that the flow rate is unit. This is physically required. Note that the mean axial velocity and the channel width are used to normalize the governing equations. The algorithm requires a trial and error procedure along with the time marching until the steady state is achieved. The advantage of this algorithm is that no assumption is needed for the entrance velocity profile.

Thermal boundary conditions are set up on the periphery of the entire domain, which are $\partial\theta/\partial y = 0$ on adiabatic walls, $\theta = 0$ at inflow boundary, and $\partial\theta/\partial x = 0$ at outflow boundary. The initial conditions are of no consequence to the steady-state solution.

The Nusselt number of the blocks is defined by $Nu_b = 1/(2h + w)\theta_{wm}$, where θ_{wm} is the average wall temperature over the surfaces of each block exposed to the fluid.

Results and Discussion

The present computation domain consists of 202 grids in x direction and 56 grids in y direction. A nonuniform grid distribution is used with dense meshes near the blocks. Meshes with fewer grids were tested to ensure grid independence. The mass and energy residues are checked for convergence in the process of marching in time. It is found that these criteria have been met long before the steady state is reached. Therefore, our problem is essentially to check whether the steady state is reached by tracing the variation of the flow and temperature distribution from the given initial state. It is to be sure that the largest variation in the whole field is reduced consistently and is kept below some specified criteria. Judging from our previous experience,[7] the steady state is considered to have arrived at when flow rate change is under 10^{-5} and the largest Nusselt number change is below 10^{-3}, at a time interval of $\Delta t = 3$. The associated computer program has also been checked with the natural convection results of Aung et al.[8] Detailed results of local Nusselt numbers, flow patterns, and isotherms for the same configuration may be found in Ref. 9.

The buoyancy-induced flow, as well as Rn, is calculated by setting the identical equivalent pressure at the entrance and the exit. Interestingly, linear correlations between Ra and the ratio Ra/Rn^2 are obtained by plotting the numerical data in a Rayleigh number range of $5 \times 10^3 \sim 4 \times 10^5$. The correlation, confirmed by arrangements of five, three, and one block, can be written as $Ra/Rn^2 = a + bRa$, where the coefficients a and b vary with geometry. For example, for the five-block arrangement, a and b are equal to 3.7379 and 6.0905 $\times 10^{-5}$, respectively. The natural Reynolds number can be solved directly from this correlation. The resulting expression has two limiting cases: when Ra is not very large, Rn scales like the square root of Ra, a well-known fact for the smooth channel with uniform wall heat flux[1]; when Ra is above 5×10^5, Rn approaches to a constant. The small coefficient b represents the shifting of velocity profile from a symmetrical one to a buoyant plume, which occurs in the calculated Ra range.

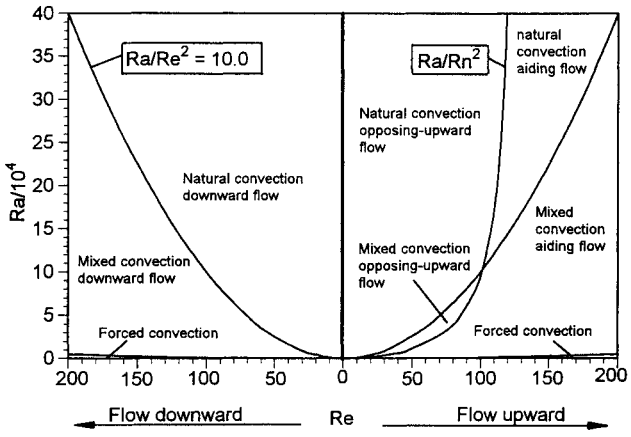

Fig. 2 Regimes of various heat transfer and fluid flow situations for present geometry of five blocks.

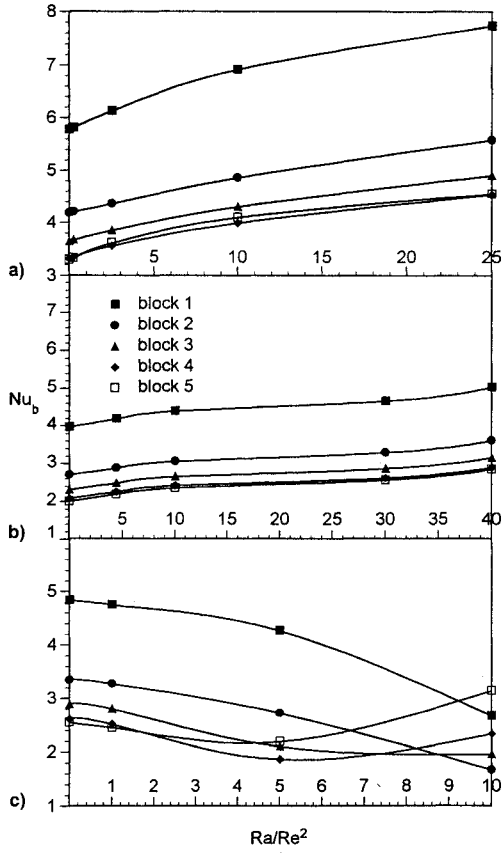

Fig. 3 Block Nusselt number for a) aiding flow (Re = 200), b) opposing-upward flow (Re = 50), and c) downward flow (Re = 100).

Figure 2 shows various regimes where different situations of convection are located. The demarcations for natural, forced, and mixed convection are roughly made by the magnitude of the ratio of Ra/Re^2. Mixed convection falls in the regime where $0.1 < Ra/Re^2 < 10.0$. Another demarcation in Fig. 2 is the Ra/Rn^2 curve, which sets up the border for aiding and opposing flow. The downward flow situation is to the left of $Re = 0$ in this figure. It is noted that an opposing flow occurs when $0 < Re < Rn$, in which buoyancy overcomes the downward forced flow and is referred to as opposing-upward flow. The global flow is still upward in this case. Mixed convection occurs in aiding flow, opposing-upward flow as well as in downward flow, but the chance it occurs in opposing-upward flow is relatively small. Note that mixed convection indicated here is different from the combined forced and buoyant flow.

Typical calculations for buoyancy-aided flow are made at Re = 200, and the Nusselt number of the blocks is plotted in Fig. 3a. In the calculated range of Ra, heat convection undergoes from forced mode to an approximation of natural mode. A 34% increase for the first block and a 38% increase for the fifth block are found as the ratio Ra/Re^2 rises from 0 to 25. The Reynolds number is fixed, and so the heat transfer increases without changing in global flow rate. One reason for such increase is the shift of velocity profile from a forced one toward a buoyant plume. The other reason is that, at higher Ra/Re^2, the mainstream penetrates into the grooves between the blocks, since buoyancy is a body force and does not tend to create recirculation in the grooves.

In Fig. 3b, an opposing-upward flow is presented for Re = 50. The minimum ratio of Ra/Re^2 for opposing flow is 4.408, which corresponds to the case of pure buoyancy-induced convection. Forced convection is included for comparison. Smaller Nusselt number than those of the aiding flow is found, because the Reynolds number is smaller. The calculated velocity distribution shows a large flow reversal appearing in the top region at a high Rayleigh number. However, it seems that the appearance of flow reversal does not cause much change in Nusselt number of the blocks.

Figure 3c shows the results of Re = 100 in downward flow case. In forced convection, Nusselt number starts high upstream and descends downstream. This trend remains for small Ra. At a higher Ra, Nusselt number starts high at the first block, goes to a minimum at some block in the middle, and then rises at downstream blocks. Buoyancy acts against the mainstream and strongly affects the local flow near the heated blocks. As Ra becomes higher, local buoyancy grows strong enough to balance out the forced flow, or even creates a local upflow. The recirculations that are confined in the grooves squeeze into the main stream. As a result, a large recirculation appears, and the flow becomes unsteady.

Conclusions

The following conclusions can be drawn from this study:

1) In a vertical channel, buoyancy induces a global flow that interacts with the forced flow, resulting in different cases of aiding flow, opposing-upward flow, and downward flow.

2) The buoyancy-induced flow is characterized by "natural Reynolds number." A linear correlation is found between Ra and Ra/Rn^2, which serves as demarcation between different flow situations.

3) Buoyancy affects the convective heat transfer from the blocks by altering the global flow and by redistributing the flow. The flow redistribution is determined by the ratio Ra/Re^2.

Acknowledgment

This study was partially supported by a Research Challenge Grant sponsored by the Ohio Board of Regents.

References

[1]Peterson, G. P., and Ortega, A., "Thermal Control of Electronic Equipment and Devices," *Advances in Heat Transfer*, Vol. 20, Academic, 1990, pp. 181–314.

[2]Jeng, Y. N., Chen, J. L., and Aung, W., "On the Reynolds-Number Independence of Mixed Convection in a Vertical Channel Subjected to Asymmetric Wall Temperature with and Without Flow Reversal," *International Journal of Heat and Fluid Flow*, Vol. 13, No. 4, 1992, pp. 329–339.

[3]Gau, C., Yih, K. A., and Aung, W., "Numerical and Analytical Study of Reversed Flow and Heat Transfer in a Heated Vertical Duct," *Mixed Convection Heat Transfer*, edited by M. Keyhani and R. Kumar, American Society of Mechanical Engineers HTD-Vol. 247, 1993, pp. 9–19.

[4]Kim, W. T., and Boehm, R. F., "Combined Free and Forced Convective Heat Transfer from Multiple Rectangu-lar Wall Blocks in Vertical Channels," *Mixed Convection and Environmental Flows*, American Society of Mechanical Engineers HTD-Vol. 152, 1990, pp.

1–8.

[5]Patankar, S. V., *Numerical Heat Transfer and Fluid Flow*, Hemisphere, New York, 1980.

[6]Leonard, B. P., "A Stable and Accurate Convective Modeling Procedure Based on Quadratic Upstream Interpolation," *Computer Methods in Applied Mechanics and Engineering*, Vol. 19, No. 1, 1979, pp. 59–98.

[7]Chung, B. T. F., and Li, H. H., "Forced Convective Cooling Enhancement of Electronic Modules Through a Double Layer Design," *Journal of Electronic Package*, Vol. 117, No. 1, 1995, pp. 69–74.

[8]Aung, W., Fletcher, L. S., and Sernas, V., "Developing Laminar Free Convection Between Vertical Plates with Asymmetric Heating," *International Journal of Heat and Mass Transfer*, Vol. 15, No. 11, 1972, pp. 2293–2308.

[9]Li, H. H., and Chung, B. T. F., "Mixed Convection in a Vertical Channel with Internally Heated Rectangular Blocks," *Fundamentals of Mixed Convection*, edited by T. Y. Chu and T. S. Chen, American Society of Mechanical Engineers HTD-Vol. 274, 1994, pp. 9–16.

Particle Drag Coefficient in Solid Rocket Plumes

H. F. Nelson* and John C. Fields†
University of Missouri–Rolla, Rolla, Missouri 65401

Nomenclature

A	=	particle cross-sectional area, $\pi d^2/4$
a	=	speed of sound in gas
C_D	=	particle drag coefficient, $2D/(\rho U^2 A)$
$(C_D)_{ave}$	=	see Eq. 7
$(C_D)_{DSMC}$	=	particle drag coefficient from direct simulation Monte Carlo
D	=	drag force
d	=	particle diameter
Kn	=	Knudsen number
M	=	freestream Mach number
Re	=	Reynolds number based on particle diameter
S	=	molecular speed ratio, $M\sqrt{\gamma/2}$
T_g, T_p	=	gas temperature, particle temperature
U	=	gas-particle relative velocity
X_i	=	mass fraction of gas i
γ	=	ratio of gas specific heats
ρ	=	gas density

Introduction

THE effect of drag on trajectories of particles in solid rocket plumes can significantly influence convective and radiative heat transfer to the base of the rocket and plume radiation signatures. In this Note we present a comparison of direct simulation Monte Carlo (DSMC) drag coefficients for particles in solid rocket plumes with predictions of four empirical drag correlations currently used in plume codes. Typically, the particles are composed of aluminum oxide and have diameters from 1 to 10 μm. Due to their small size they exist in a rarefied flowfield at altitudes greater than about 40 km. Particle Kn vary from 0.5 to 1000, or larger. The plume gas temperatures are of the order of 2500 K in the core and 200 K at the outer edge. Gas-particle relative velocity can vary by up to ± 5000 m/s. Also, the composition of the plume is a mixture of many gases including H_2O, H_2, N_2, O_2, OH, NO, H, O, CO, CO_2, Cl_2, and Cl, as well as others.

DSMC Method

The DSMC method was developed by Bird[1–4] for applications to low density flow for Kn ranging from 0.025 to 100. For $Kn < 0.025$ the flow is continuum, for $Kn > 100$ the flow is free molecule. DSMC considers a number of simulated molecules, each representing a large number of real molecules. The motion of the molecules is computed in the region surrounding the particle. Molecular paths between collisions are calculated exactly, but collisions are treated statistically. Molecular motion is stopped while collisions are computed statistically throughout the entire flowfield. Next, the molecules are allowed to move in their new directions with their new velocities for a short time and then held motionless in their new positions, while another collision cycle takes place. The collisions are computed by statistical sampling. Accurate, steady-state values of flowfield properties and body-forces are obtained by continuing the calculations for a long period of time while computing a cumulative average of instantaneous samples taken at time intervals large enough to prevent correlation between successive averages. The drag coefficient is calculated from the DSMC normal and shear forces per unit area on the particle assuming complete accommodation and diffuse reflection.

Drag Correlation Equations

A brief description of each drag correlation considered in this study is provided here for convenience. The correlations are evaluated for specific individual gases in the calculations.

1) *Hermsen*: Hermsen[5] correlated C_D data for slip through free molecule flow at subsonic through supersonic velocities. Hermsen's equation is

$$C_D = 2 + (C_{D0} - 2)\exp[-3.07\sqrt{\gamma}(M/Re)\zeta] + \omega/(M\sqrt{\gamma})\exp[-Re/(2M)] \quad (1)$$

where $C_{D0} = 24[1 + 0.15Re^{0.687}]/Re$, $\zeta = [1 + (12.278 + 0.584Re)Re]/[1 + 11.278Re]$, and $\omega = 1.7\sqrt{T_p/T_g} + 5.6/(M + 1)$.

2) *Henderson*: Henderson[6] developed a drag correlation for continuum, slip, transition, and free molecule flow, which includes effects of gas-particle temperature differences. It consists of three equations. One for subsonic flow, one for supersonic flow ($M > 1.75$), and a bridging equation between the subsonic and supersonic regimes, valid for $1.0 < M < 1.75$. For subsonic flow, C_D is given by

$$C_D = \frac{24}{Re + S[4.33 + \Phi\exp(-0.247Re/S)]} + [\Psi + 0.1M^2 + 0.2M^8]\exp[-M/(2\sqrt{Re})] + 0.6S[1 - \exp(-M/Re)] \quad (2)$$

where

$$\Phi = \frac{3.65 - 1.53T_p/T_g}{1 + 0.353T_p/T_g}$$

$$\psi = \frac{4.5 + 0.38(0.03Re + 0.48\sqrt{Re})}{1 + 0.03Re + 0.48\sqrt{Re}}$$

Received Feb. 10, 1995; revision received March 10, 1995; accepted for publication March 10, 1995.

*Professor of Aerospace Engineering, Department of Mechanical and Aerospace Engineering and Engineering Mechanics. Associate Fellow AIAA.

†Graduate Student, Department of Mechanical and Aerospace Engineering and Engineering Mechanics.